Top Curr Chem (2003) 225: 207–232
DOI 10.1007/b10470

Gas-Phase Conformations: The Ion Mobility/Ion Chromatography Method

Thomas Wyttenbach[1] · Michael T. Bowers[2]

Department of Chemistry and Biochemistry, University of California at Santa Barbara, Santa Barbara, California 93106, USA
[1] *E-mail: wyttenbach@chem.ucsb.edu*
[2] *E-mail: bowers@chem.ucsb.edu*

Ion mobility spectrometry coupled to mass spectrometry provides a powerful tool to explore the three-dimensional shape of polyatomic ions. Applications include the investigation of cluster ion geometries and conformations of flexible molecules such as biopolymers and synthetic polymers. The ion structure is obtained by measuring collision cross sections in a high pressure drift tube filled with helium and comparing it to model structures obtained by various theoretical methods such as molecular modeling and electronic structure calculations. The temperature of the drift tube is generally adjustable (typically from 80 to 800 K) providing a unique opportunity to address topics such as the thermal motion of floppy molecules, the unfolding process of folded structures, the kinetics of structural interconversion, and the kinetics of dissociation processes. In addition, the ion mobility instrumentation can be used to obtain thermochemical data of ligand addition reactions, giving important additional information about the polyatomic ions under investigation. The theoretical background and the concepts of these ion mobility based experiments and the instrumentation employed are briefly reviewed in this chapter. Furthermore, some detailed examples and a very brief summary of selected applications found in the literature are given.

Keywords. Molecular geometry, Polymer, Protein, Peptide, Cluster

1 Introduction 209

2 Concepts 210

2.1 Ion Mobility and Cross Section 210
2.2 Model Structures 211
2.3 Kinetic and Thermochemical Data 211

3 Instrumentation 212

3.1 Basic Setup 212
3.2 Temperature Controlled Drift Cell 213
3.3 High Resolution Drift Tube 214
3.4 Two-Dimensional Mobility-Mass Data 215

4 Methods and Examples 216

4.1 Cross Sections: Experiment and Theory 216
4.2 Kinetics 217
4.2.1 Serine Clusters 217
4.2.2 Bradykinin Dimer 219

4.2.3 PET Trimer 220
4.3 Equilibrium: Ligand Binding Energy 222

5 Overview of Applications 224

5.1 Conformations of Flexible Molecules 224
5.2 Geometries of Clusters 226

6 Conclusions 228

7 References 229

List of Abbreviations and Symbols

A	Arrhenius pre-exponential factor
Ac	Acetyl
ala	Alanine
arg	Arginine
argOMe	Arginine methyl ester
ATD	Arrival time distribution
BPTI	Bovine pancrease trypsin inhibitor
e	Electric charge
E	Electric field
E_a	Arrhenius activation energy
ESI	Electrospray ionization
FT-ICR	Fourier transform ion cyclotron resonance
gly	Glycine
IMS	Ion mobility spectrometry/spectrometer
K	Ion mobility
k	Rate constant
k_B	Boltzman constant
K_{eq}	Equilibrium constant
LHRH	Luteinizing hormone releasing hormone
lys	Lysine
m/z	Mass to charge ratio
MALDI	Matrix assisted laser desorption ionization
MD	Molecular dynamics
MM	Molecular mechanics
MS	Mass spectrometry/spectrometer
N	Particle number density
p	Pressure
PET	Poly(ethylene terephthalate)
POSS	Polyhedral silsesquioxone
pro	Proline
ser	Serine
SIFDT	Selected ion flow drift tube
T	Temperature

t_D	Drift time
TOF	Time of flight
u	Atomic mass unit
val	Valine
v_D	Drift velocity
V_D	Drift voltage
$\Delta H°$	Standard enthalpy change
$\Delta S°$	Standard entropy change
Δt_D	Drift time spread
μ	Reduced mass
σ	Cross section

1 Introduction

This chapter is a brief summary of recent advances in the field of ion mobility–mass spectrometry (IMS-MS) used to obtain structural information of ionic species such as the conformations of biological molecules and the three-dimensional arrangement of atoms in cluster ions. Such IMS-MS applications typically include extensive theoretical work for generating reasonable model structures of the molecular systems studied experimentally, as it is really the synergics of experiment and theory that provides detailed information on molecular structure using the ion mobility technique (or ion chromatography technique as it is sometimes called in this context to set it apart from conventional IMS applications). We will review the concepts and instrumentation used to obtain molecule structure information by IMS-MS and demonstrate the methods on a number of examples. Finally, we will attempt to summarize the major conclusions obtained from the body of work, that emerged in the past five years. IMS applications simply to separate ions of different mobility, generally analytical in nature, are not included in this work. Further, we are not attempting to be totally exhaustive in the review and have chosen detailed examples primarily from our own work, much of which is unpublished at this time.

The area of ion mobility research to obtain structural information started to emerge in the early 1990s and was pioneered by the groups of Bowers [1–5] and Jarrold [6, 7]. Most of the early work was reviewed by Clemmer and Jarrold [8] in 1997 and we focus here on the work that has appeared since then. One major point of interest in the field is clearly the structure of biological molecules in the presence and absence of solvation molecules. Molecules as small as glycine and as large as cytochrome *c*, a heme protein composed of more than 100 amino acids, were studied to address issues such as zwitterion formation in peptides, proteins, and oligonucleotides; protein folding; peptide helix formation; the dynamics of interconversion between conformations; and the effects of hydration. Other significant results were obtained for synthetic polymers, for nonmetal, semiconductor, and metal clusters, and for salt and ion-molecule clusters. In Sect. 5 we will give references to these recent applications together with a short overview of the major conclusions.

2 Concepts

2.1 Ion Mobility and Cross Section

Ions drifting through a buffer gas under the influence of a weak uniform electric field E quickly reach an equilibrium between forward acceleration due to the electric field and retarding effect due to collisions with the buffer gas resulting in a constant drift velocity v_D. The drift field is weak when the steady flow of ions along the electric field is much slower than the random motion leading to diffusion. The low field mobility K is the proportionality constant between v_D and E [9]:

$$v_D = KE\,. \tag{1}$$

Hence, measuring the drift time t_D for a given drift length and given E yields an experimental value for K. For a given pressure (or particle density N) and temperature T of the buffer gas the ion mobility K is given by the collision cross section σ by

$$K = \frac{3e}{16N}\left(\frac{2\pi}{\mu k_B T}\right)^{1/2}\frac{1}{\sigma} \tag{2}$$

where e is the charge of the ion, μ the reduced mass of ion and buffer gas, and k_B the Boltzman constant [9]. Thus, ions with compact structures have a small cross section and a large ion mobility, whereas the opposite is true for large extended structures. Hence, in ion mobility spectrometry (IMS) ions are separated (therefore the term "ion chromatography") by size (collision cross section) in contrast to mass spectrometry, where they are dispersed by mass (mass to charge ratio). The collision cross section is not only determined by the geometry of the ion but also by the interaction between ion and buffer gas. This is particularly true for small ions, large and polarizable buffer gases, and at low temperatures. Therefore, helium is the buffer gas of choice for obtaining structural information by ion mobility techniques and it is the only buffer gas used in all the work reviewed here.

While it is straightforward to measure an experimental collision cross section via drift time and ion mobility, it is far more difficult to obtain a reliable value for a given model structure for comparison with experiment. A number of models have been proposed to calculate theoretical cross sections. A simple approach is to calculate an orientation averaged projection cross section of the model geometry using hard spheres with a specified radius for each atom in the system. In sophisticated methods the radii are adjusted as a function of temperature and ion size (number of atoms) on the basis of ion–buffer gas interaction potentials, which are generally of a (12, 6, 4) form [10, 11]. For small ions with less than 200 atoms and using He as buffer gas the projection approximation agrees with the ion mobility experiment rather well [10–12]. However, it obviously fails to describe the scattering process that is actually taking place in the experiment, and it is momentum transfer that determines the collision cross section. Hence, models based on calculating collision integrals using trajectory calculations [13]

are potentially more accurate. Again, for smaller ions with several hundred atoms the ion-buffer gas interaction has to be treated accurately, usually with a (12, 6, 4) potential, in order to get good agreement with experiment and to get a reasonable temperature dependence. For larger ions (e.g., proteins) the interaction potential is much less important and a hard sphere scattering model yields very good results [14]. Other models including scattering from an iso-electron density surface are presently also being used [15].

2.2 Model Structures

Generating model structures of the ionic molecular species under investigation is essential for interpreting ion mobility data. Computational methods are generally used to obtain candidate model geometries, although crystal structures obtained by X-ray crystallography and solution structures obtained by nuclear magnetic resonance techniques are sometimes useful as well. Molecular mechanics/molecular dynamics (MM/MD) is often the method of choice for calculations because the size of the systems does not allow use of higher level theories. MM is also used for smaller systems to thoroughly search conformational space. However, MM methods are limited to systems where empirical force field parameters are available, i.e., systems composed of elements typically found in organic molecules. For all other types of systems ab initio and density functional calculations are an alternative. However, because of limitations to computer power geometry optimization using such electronic structure calculations are only possible for smaller systems, typically in the range of tens of atoms. Hence, the only possibility for large systems with organically atypical atoms is to parameterize the atypical atom(s) for inclusion in standard force fields. An example of this procedure is parameterization of the silicon atom for use in the AMBER [16] force field allowing MM/MD calculations on polyhedral silsesquioxone (POSS) polymers [17, 18].

2.3 Kinetic and Thermochemical Data

The ion drift tube setup used to measure ion mobilities can also be used to obtain kinetic and thermochemical data often providing important information about the ion under investigation in addition to the collision cross section. If a chemical reaction like an isomerization (change in cross section) or a dissociation (change in cross section or mass to charge ratio) occurs on the time scale of the experiment a reaction rate constant can be measured precisely, since the reaction time (i.e., the drift time) and the temperature are both well defined and readily measured. In addition, since the drift tube temperature can be changed, an Arrhenius type of analysis yields activation energies and pre-exponential factors for the reaction. More details and examples for such experiments are given in Sect. 4.2.

If the time scale of a chemical reaction is much shorter than the experimental time scale a chemical equilibrium will be established. However, an isomer-

ization equilibrium cannot be studied on the basis of cross section (even if different isomers have different cross sections), because the fraction of time an ion travels as one isomer or the other is the same for each ion and therefore every ion exhibits the same cross section, an average of all interconverting isomers.

However, an equilibrium between products and reactants that have different mass to charge ratios can be examined by means of mass spectrometry at the exit of the drift tube. In such an equilibrium, care has to be taken that products and reactants, including any non-ionic species, are present with defined concentrations. The type of equilibrium typically studied using this technique are reactions where ligands are added to ions which were injected into the drift tube. In this case the neutral ligand is present in the drift cell with a defined pressure. Such reactions include ligation of metal ions and solvation of ions by solvent molecules. Studying an equilibrium as a function of temperature yields $\Delta H°$ and $\Delta S°$ values for the reaction in question. Details and an example of this type of experiment are given in Sect. 4.3.

3 Instrumentation

3.1 Basic Setup

The basic setup allowing for most flexibility to carry out ion mobility experiments is schematically depicted in Fig. 1. Ions are generated in an ion source, mass selected in a first mass filter MS1, and injected into the drift tube. If the ion source produces a continuous ion beam, the beam has to be gated in front of the drift cell, the gate triggering the clock for measuring the drift time of the ion pulse. Sophisticated equipment like a quadrupole ion trap [19–21] or an ion funnel [22] can be used as a gate and ion storage device to convert a continuous ion beam into a pulsed one without significant ion loss.

Ions exiting the drift tube are mass analyzed in mass spectrometer MS2, an important feature if reactions are occurring in the drift cell. Ions are generally detected after MS2 by ion counting techniques. The mass spectrometers MS1 and MS2 are typically quadrupole mass filters, and either one or the other can be run in RF-only mode for better signal but without mass selection, if desired.

The setup in Fig. 1 is conceptually not new. It has been used for decades by a number of groups [23–26] after pioneering work of Hasted and coworkers in 1966 [27]. Also the selected ion flow drift tube (SIFDT) technique [28–33] emerging in the 1980s by combining the features of a drift tube with a flowing afterglow apparatus [34] is equivalent to the setup in Fig. 1. However, all of the

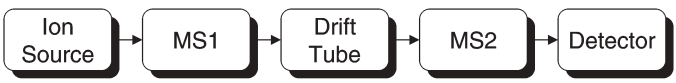

Fig. 1. Schematic outline of the basic ion mobility–mass spectrometry setup using mass selection before (MS1) and after (MS2) the drift tube

instrumentation employed in these earlier studies was used to examine the chemistry and the interaction of various small, often atomic ions with various buffer gases, and a large part of this research was geared towards understanding atmospheric ion chemistry processes.

Injecting ions into a drift tube becomes increasingly more difficult with increasing drift tube pressure. However, high drift tube pressure is desirable for high ion mobility resolution. For these reasons omitting MS1 is a common simplification of the basic setup in Fig. 1 and is typically found in analytical IMS-MS [35] and other high pressure drift tube applications (see Sect. 3.3) [36].

As mentioned above, the mass spectrometers MS1 and MS2 are often quadrupole mass filters, but other types of mass spectrometers have been coupled to IMS as well, including magnetic sectors [37], FT-ICR [38], quadrupole ion trap [21] and time of flight (TOF) mass spectrometers [39–45]. TOF-MS has the advantage that there are no theoretical limits to the mass to charge ratio (*m/z*) covered, whereas quadrupoles typically operate up to a maximum *m/z* of several thousand mass units. Hence, TOF-MS delivering pulses of mass dispersed ions, one of which can be selected by an ion gate, works very naturally as a front end (MS1) to the drift cell to study ions with very high *m/z* values. In this setup a pulsed ion source, such as MALDI, is an ideal choice [45]. Another important feature of TOF-MS is that ions of different *m/z* are non-destructively dispersed in time and not in space like in quadrupole filters, where non-selected ions are lost due to unstable trajectories. Therefore, coupling a TOF-MS to the exit of the drift tube is particularly interesting (MS2) and yields a setup that allows one to obtain two-dimensional mobility-mass information theoretically within seconds (see Sect. 3.4) [39–44].

3.2 Temperature Controlled Drift Cell

Most drift cells used in the applications outlined in this article can be temperature controlled to some degree. In this section we describe the basic design of Kemper and Bowers [22, 37, 46] as an example of a drift cell that is very suitable for applications where high ion transmission of several percent and adjustable temperatures within a large range from typically 80 K (liquid nitrogen) to 800 K are desirable. The upper temperature limit is given by the materials used and by the mechanical design providing a uniform temperature distribution and allowing for expansion of the material at high temperatures.

The temperature controlled drift cell shown in Fig. 2 is fabricated from a copper block with the ring electrodes (providing the drift field) in the interior of the cell. Heating is provided by electrical heaters inserted from the outside into bores in the copper cell. Cooling is achieved by running a pre-cooled gas (typically nitrogen cooled in liquid nitrogen) through a set of bores in the cell block that makes up a cooling cycle. The resistor chain connecting the ring electrodes can be either run in the interior (preferred) or exterior (using feedthroughs) of the cell. The ring electrodes are spaced by ceramic spacers on ceramic rods and by springs to allow for temperature affected contraction and expansion.

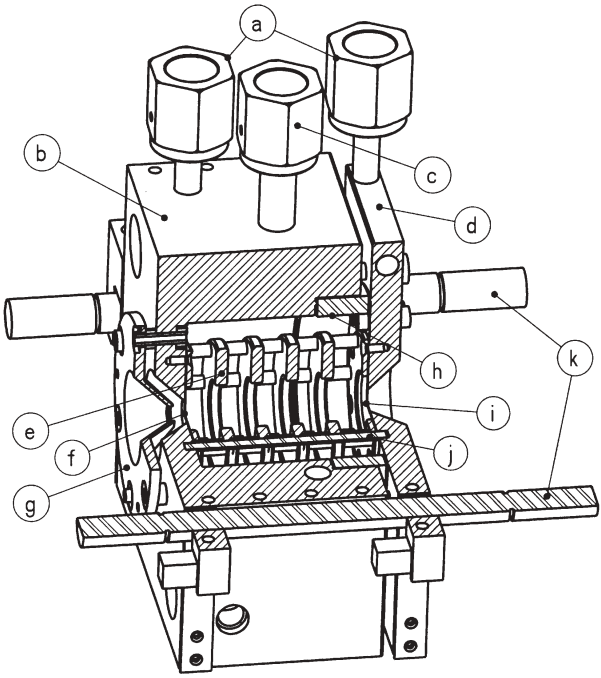

Fig. 2. Perspective cross sectional view of the temperature controlled drift cell after Kemper and Bowers' design [22]: (a) cooling line, (b) cell body, (c) buffer gas inlet, (d) cell end cap, (e) drift guard ring, (f) ion entrance hole, (g) ion focusing lens, (h) ceramic ring, (i) ion exit hole, (j) ceramic rod holding guard rings, (k) ceramic rods holding cell assembly

The ion entrance plate (~0.1 mm thick) with a small hole (typically 0.5 mm diameter) has the same electric potential as the copper cell, whereas the exit plate (same dimensions) is mounted to a cell end cap that is electrically isolated from the cell body by a ceramic ring. The end cap has its own cooling and heating systems.

The entire cell assembly is supported by two large ceramic rods running left and right of the cell parallel to and on the same height as the ion beam. The cell assembly is self-centered between the two rods by a leaf-spring setup that also allows for expansion and contraction of the assembly.

This cell is typically 4–5 cm long and operates at pressures of 3–5 torr and drift voltages of 10–100 V across the cell.

3.3 High Resolution Drift Tube

The resolution $t_D/\Delta t_D$ of a drift tube is proportional to the square root of the drift voltage V_D across the tube [9]:

$$\frac{t_D}{\Delta t_D} = \left(\frac{\pi e V_D}{4 k_B T}\right)^{1/2} \tag{3}$$

where t_D is the average drift time, Δt_D the drift time spread due to diffusion, e the ion charge, k_B the Boltzman constant, and T the temperature. Hence, to increase resolution it is desirable to increase V_D, while still fulfilling the weak field condition (see Sect. 2.1). This is achieved in two ways: by increasing the drift length and by increasing the pressure. In the design used in Jarrold's laboratory and briefly described below, a drift voltage V_D of up to 15,000 V can be used by employing a pressure of 500 torr and a tube that is 63 cm long [36]. Since ions cannot be injected from vacuum into a drift tube maintained at such high pressures, mass selection prior to the high resolution drift tube is not possible. Ions are formed immediately in front of the tube at high pressure and pulled into the drift region through an "ion gate". The ion gate prevents neutral species from entering the drift tube by a counter flow of helium and carries ions through by an electric field.

The high resolution drift tube is fabricated from a six-inch diameter steel tube divided into three sections separated by ceramic breaks. The field in the interior is maintained by copper beryllium drift guard rings, connected to each other by a resistor chain. In Jarrold's apparatus [36] the ion exit hole has a diameter of 0.13 mm. The drift tube temperature is controlled by jackets around each section and by a recirculator with non-conducting temperature regulated fluorocarbon fluids.

Similar drift tubes with similar dimensions are used as medium resolution devices employing a V_D of several hundred to 1000 V and pressures of several torrs [39]. In this lower pressure, medium resolution setup ions are generally injected into the drift tube from vacuum, often with mass selection prior to the drift tube.

3.4 Two-Dimensional Mobility-Mass Data

In this section we would like to point out one of the many possible ion mobility-mass spectrometer combinations, that appear to make up a particularly intriguing setup, the drift tube–TOF-MS combination [39–44]. In this setup shape separated ions exiting the drift tube are further dispersed in time by their mass to charge ratio. The timing works out such that ions are first shape separated on a several millisecond time scale and subsequently mass-to-charge separated on the fly on a 10-μs time scale [39]. Thus pulses of ions are injected into the drift tube at a repetition rate of the order of 10 Hz and ions exiting the drift tube are injected into the TOF-MS at a repetition rate of 10^4 Hz. Timing is one of the reasons why the ion mobility-TOF-MS combination works so well together, but it is also the fact that both techniques work with ion pulses and that TOF is not a scanning technique, where all ions are lost except for those with the m/z value selected. However, coupling ion mobility to TOF-MS is technically challenging as nearly ten orders of magnitude of pressure difference between drift tube and TOF-MS have to be overcome. In addition, optimizing the duty cycle of pulsing ions into the TOF-MS is critical for getting good data in a short period of time [47], otherwise long signal accumulation times counteract the extraordinary time advantage gained by TOF-MS.

4
Methods and Examples

4.1
Cross Sections: Experiment and Theory

As mentioned in Sect. 2.1 the mobility measurement of a polyatomic ion provides a value for its orientation averaged cross section and hence information about its shape. Extended, elongated structures of a given molecule have larger rotationally averaged cross sections than compact more spherical structures. For instance, the projection cross section of a right-handed α-helix of the peptide (gly-ala)$_7$Cs$^+$, an extended structure (Fig. 3b), is expected to be 243±10 Å^2, whereas that of a globular, near spherical structure of the same molecule is of the order of 213±5 Å^2 (Fig. 3a) [48]. Most of the "error" bars indicated with these values are due to geometry changes as a function of time during thermal motion at 300 K. The models in Fig. 3 have been obtained by molecular modeling calculations using the AMBER force field [16]. It is of interest that globular structures are only stable if the cesiated (gly-ala)$_7$ peptide is assumed to be a zwitterion. As soon as the proton is transferred from the N-terminus (NH_3^+–) to the C-terminus (–COO–) the peptide prefers to fold into a 95% α-helical conformation, where Cs$^+$ caps the helix on the C-terminus side. If Cs$^+$ is replaced by smaller alkali ions more globular charge solvation structures become competitive compared to the helix. An analysis of the Ramachandran plot for a typical (gly-ala)$_7$Li$^+$ charge solvation structure indicates that only 23% is α-helical, just like the protonated form (gly-ala)$_7$H$^+$ (26% helical, σ=213 Å^2). The sodiated, potas-

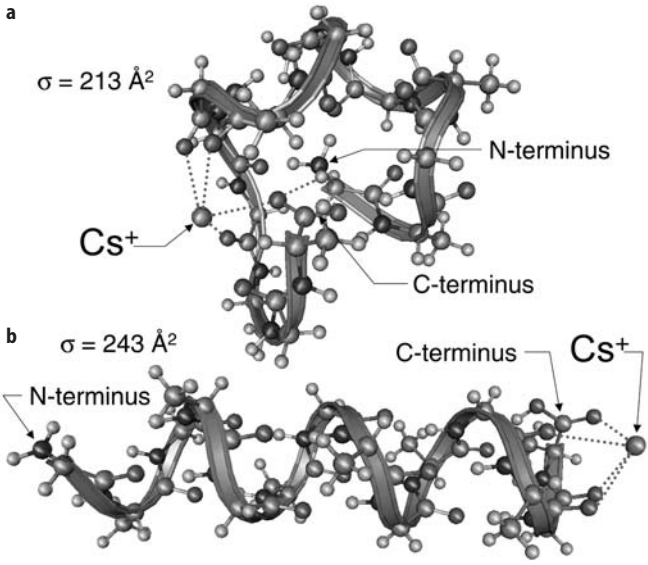

Fig. 3a, b. Structures of (gly-ala)$_7$Cs$^+$ obtained by molecular mechanics calculations: **a** globular zwitterion structure; **b** α-helical non-zwitterion structure

siated, and rubidiated peptides yield conformations which are 59%, 77%, and 90% helical, respectively. The zwitterionic structures for all alkali ions are compact and <20% helical.

Thus, this type of system is ideally set up to be explored by ion mobility. Experimental cross sections for all of the $(gly\text{-}ala)_7X^+$ systems, $X^+=H^+$, Li^+ through Cs^+, are in the range of 211–216 Å^2 at 300 K [48] thus ruling out extensive helix formation for any of the systems. For $(gly\text{-}ala)_7H^+$ the experiment (216±5 Å^2) is in agreement with theory which predicts a non-helical compact charge solvation structure (213 Å^2). For the alkali ion cationized systems both globular and helical conformations are theoretically plausible. However, the experiment indicates that globular structures win out for all alkali ions. For the small alkali ions both compact charge solvation and zwitterion structures are potential candidates. For Cs^+ globular charge solvation structures can be ruled out on theoretical grounds, since they are expected to be less stable than an α-helix by more than 10 kcal mol^{-1}. Hence, experiment leads to the conclusion that the structures of the $(gly\text{-}ala)_7X^+$ are all similar for any choice of X^+ ($X^+=H^+$, alkali ion). However, the combination of experiment and theory makes structural assignments possible and leads in this case to the conclusion that all the structures are non-helical and that the cesiated peptide assumes a compact zwitterion structure.

4.2 Kinetics

If an ion injected into the drift tube is undergoing a reaction from one species with cross section A to another one with cross section B≠A during the drift time, the cross section measured for that ion is between A and B. An ensemble of reacting ions gives a cross section distribution ranging from A (late or no reaction) to B (early reaction). Using kinetic theory the expected cross section distribution for such a system can be calculated for given A, B, and reaction rate constant [49]. Therefore, the only unknown parameter, the rate constant, can be obtained by fitting the theoretical distribution to experiment.

It should be emphasized that the reaction is occurring under thermal conditions at a temperature defined by the helium buffer gas. Measuring rate constants k as a function of temperature yields activation energies E_a and pre-exponential factors A for the reaction, assuming Arrhenius-type behavior:

$$k = Ae^{-E_a/k_B T} \tag{4}$$

Below we will discuss three examples of reactions that have been studied using ion mobility instrumentation. The first example is a dissociation with loss of a neutral fragment (decrease of m/z), the second example is a dissociation where both fragments have identical m/z, and the third example is an isomerization.

4.2.1 *Serine Clusters*

Recent ESI studies of serine showed extensive formation of singly or multiply protonated clusters $(ser)_nH_z^{z+}$ (Fig. 4a) [50–54]. In many cases "magic" numbers

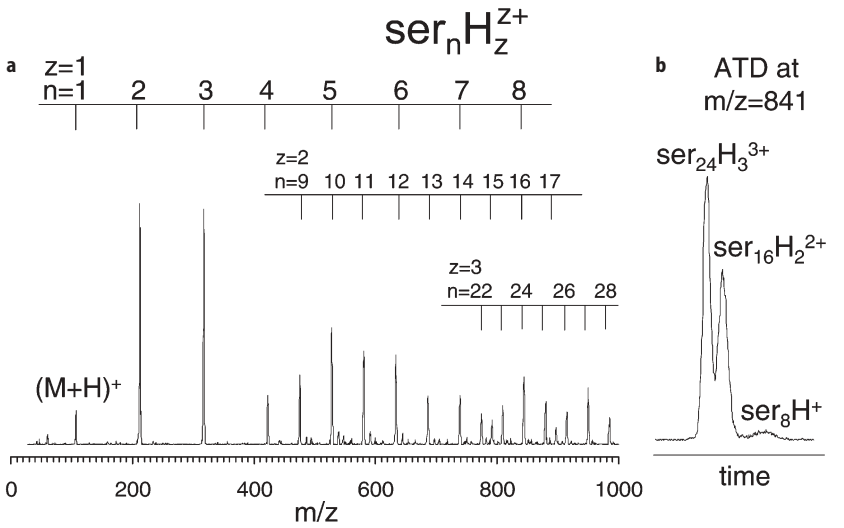

Fig. 4. **a** Electrospray mass spectrum of a 100 mmol l^{-1} solution of L-serine; extensive clustering of serine units is observed for charge states z=1, 2, and 3. **b** Ion mobility spectrum of ions with m/z=841 showing the three features assigned as protonated octamer, doubly protonated 16-mer, and triply protonated 24-mer

for *n* have been reported in the literature. The presence [50–53] or absence [54] (Fig. 4) of "magic" numbers appears to be strongly dependent on source conditions. The mass spectrum shown in Fig. 4a shows a smooth distribution of singly, doubly, and triply protonated clusters. The ion mobility spectrum (or ion arrival time distribution, ATD) recorded at constant m/z=841 (Fig. 4b) indicates the presence of three features, that can readily be assigned as $(ser)_8H^+$, $(ser)_{16}H_2^{2+}$, and $(ser)_{24}H_3^{3+}$ [54].

If serine clusters are injected into an ion mobility cell held at elevated temperature the clusters dissociate. Figure 5a shows mass spectra obtained with source conditions that produce only the small clusters $(ser)_nH^+$, *n*=1, 2, 3, which are injected into the drift cell maintained at the temperature indicated [54]. It can be seen that the trimer dissociates just above room temperature and disappears from the mass spectrum recorded after the ions have left the drift cell. The ion mobility spectrum recorded at an m/z of 211 (serine dimer) at 334 K (Fig. 5b) shows that there is a slow component at longer drift times stemming from the larger trimer that dissociated during the drift time into the dimer. At 464 K there is a slow component for m/z=106 (Fig. 5c) indicating that the dimer is dissociating into the monomer at this temperature. Analyzing the ion mobility and mass spectra as a function of temperature yields a trimer dissociation threshold of ~4 kcal mol^{-1}. The dimer is much more stable and dissociates only at temperatures near 450 K and above. The dimer binding energy is determined to be ~20 kcal mol^{-1}.

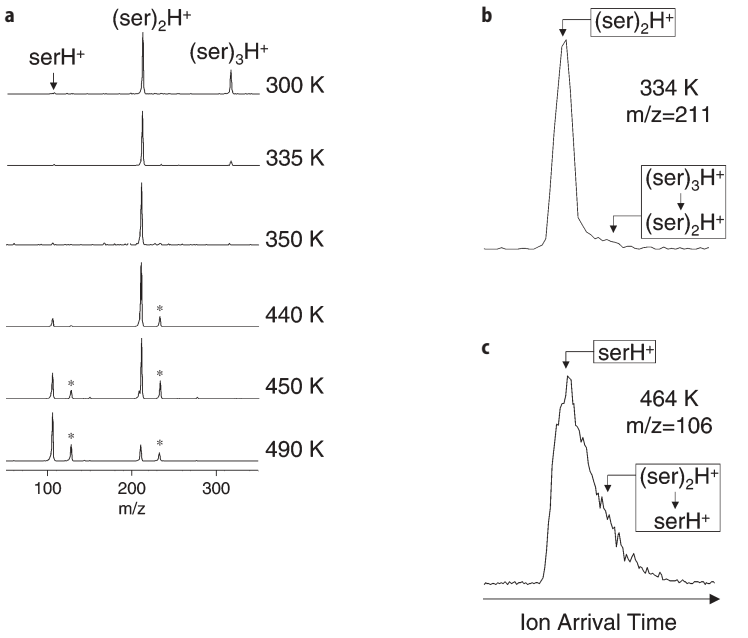

Fig. 5. **a** Mass spectra of L-serine obtained after ions spent ~200 μs in the drift cell at the temperature indicated. With increasing temperature first the trimer $(ser)_3H^+$ and then the dimer $(ser)_2H^+$ disappear from the spectrum; Relative intensities of peaks corresponding to sodiated species (marked with *) are not reproducible. **b** 334 K ion arrival time distribution (ATD) of dimer ions exiting the cell (m/z=211). **c** 464 K ATD of serine monomer (m/z=106)

4.2.2 *Bradykinin Dimer*

It has been found by ESI mass spectrometry techniques that singly protonated small peptides tend to form aggregates of the type $(nM+nH)^{n+}$ [22, 55–59]. Dissociation of such aggregates into smaller units can be studied by ion mobility techniques. Figure 6 shows ion mobility data for m/z=1061 of bradykinin recorded at different temperatures [22]. The two large features present at 441 K are the monomer $(M+H)^+$ and the dimer $(2M+2H)^{2+}$ with identical m/z=1061 ratio. The dimer feature disappears from the spectrum at a temperature of >500 K. The data at 463 K shows a fill-in between the monomer and dimer feature indicating that dissociation is occurring during the drift time. A fraction of the dimer ions, starting out with the larger dimer mobility, converted into two monomer units drifting for the remaining time with a smaller monomer mobility. The $(M+H)^+$ mobility is smaller than the $(2M+2H)^{2+}$ mobility because the ion mobility is proportional to the charge. Therefore singly charged ions drift half as quickly as doubly charged ions of same size. However, the dimer does not have the same size as the monomer, but the cross section is apparently less than twice that of the monomer ($2^{2/3}$ is expected for a sphere).

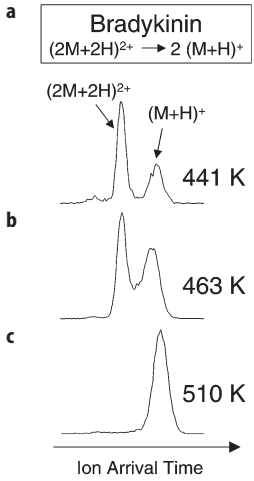

Fig. 6a–c. Ion mobility spectra of bradykinin ions at m/z=1061: **a** the two features seen at 441 K are the singly protonated monomer $(M+H)^+$ and the doubly protonated dimer $(2M+2H)^+$; **b** at a cell temperature of 463 K the dimer dissociates into two monomer units accounting for the fill-in between the two peaks; **c** at 510 K all of the dimer ions have disappeared upon exiting the cell

Fitting theoretical ion arrival time distributions to the experimental data where the rate constant for dissociation is the only adjustable parameter yields the Arrhenius plot shown in Fig. 7. The resulting dimer binding energy is ~30 kcal mol^{-1} and the pre-exponential factor is ~10^{17} s^{-1}.

4.2.3
PET Trimer

PET, poly(ethylene terephthalate), the primary constituent of a commonly used type of plastic, is composed of the rigid planar terephthalic acid units ($HOCO–C_6H_4–COOH$), which are esterified with the flexible ethylene glycol links ($HOCH_2–CH_2OH$):

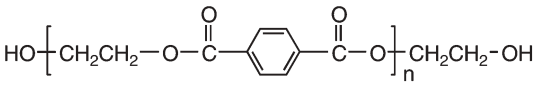

In a typical MALDI mass spectrum of PET samples a series of equally spaced peaks can readily be assigned as $[HO–(C_{10}H_8O_4)_n–C_2H_4OH]Na^+$ [60, 61]. Tuning the mass spectrometer to one oligomer size, n=3, and injecting these ions into the ion mobility cell at 300 K yields one narrow peak in the ion mobility spectrum (Fig. 8, left panel). The corresponding cross section is 175 $Å^2$. This value is right in between the values obtained theoretically for two plausible families of low energy conformations (164 and 182 $Å^2$) calculated by molecular mechanics

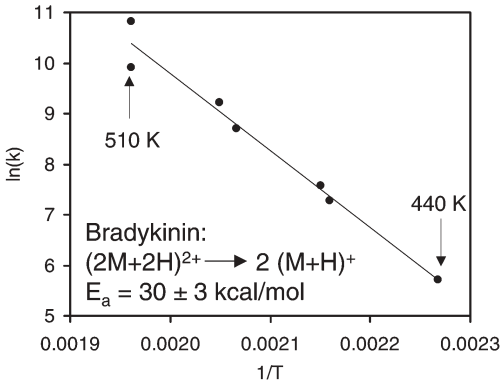

Fig. 7. Arrhenius plot for the dissociation of bradykinin dimer ions $(2M+2H)^{2+}$. Rate constant k in s^{-1}, temperature T in K

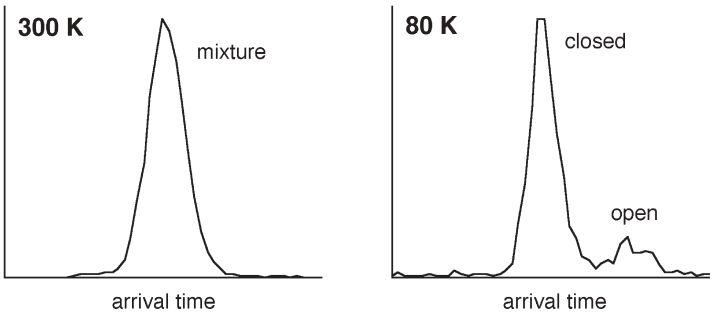

Fig. 8. Ion arrival time distributions of the sodiated PET trimer. The closed and open geometries (see Fig. 9) interconvert rapidly at 300 K (*left*), but are frozen out at 80 K (*right*)

techniques [60]. Typical representatives of the two families are shown in Fig. 9. In the closed structure (164 $Å^2$) the sodium ion is bound to oxygen atoms of both terminal $–COOC_2H_4OH$ groups, whereas this is not the case in the open (182 $Å^2$) form. In both families two of the three rigid π-systems stack up, whereas the third one is either bent in towards the sodium ion (closed structure) or extends out away from the sodium ion (open structure).

The 80 K ion mobility spectrum, shown in the right panel of Fig. 8, exhibits two distinct features, which are readily assigned to the two families of closed and open structures [60]. This means that interconversion between the two families of structures is frozen out at 80 K, but is rapid at 300 K. Data taken between 110 and 190 K show that the two peaks present at low temperature melt into one at higher temperatures. Analysis analogous to the previous examples yields an activation barrier for the open-to-closed conversion of 1.6 kcal mol^{-1}. The open-to-closed reaction turns on more rapidly than the reverse reaction, and the closed form is found to be ~0.5 kcal mol^{-1} more stable than the open form [60].

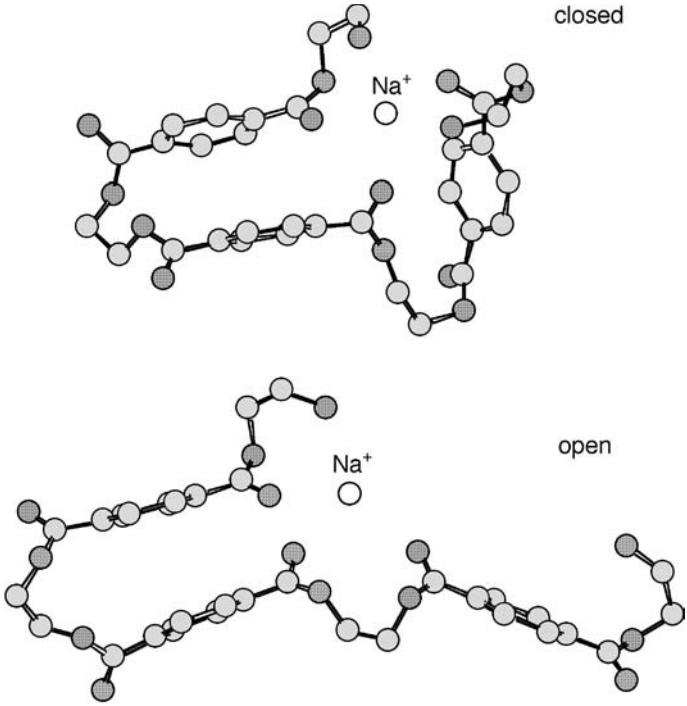

Fig. 9. Closed and open structure for the sodiated PET trimer obtained by molecular modeling

4.3 Equilibrium: Ligand Binding Energy

Ion mobility equipment can be used to obtain precise thermochemical data. The concepts briefly outlined in Sect. 2.3 are here applied to the example of hydration of protonated arginine methyl ester (argOMe)H^+. Molecular mechanics calculations indicate that the water molecule only binds to the guanidinium group and not (simultaneously) to any of the other functional groups [62]. Therefore, (argOMe)H^+ is a good model compound to measure the intrinsic binding energy of water bound to a guanidinium group in an arginine residue of a peptide or protein.

In the experiment the (argOMe)H^+ ions are formed by ESI and injected into an ion mobility cell, which is filled with a defined pressure of water of 0.1–2 torr [22, 62]. The ions undergo collisions with water molecules and an equilibrium of the form

$$(\text{argOMe})H^+ + H_2O \rightleftharpoons (\text{argOMe})H^+ \cdot H_2O \qquad (5)$$

is established. Product and reactant ions are analyzed by recording a mass spectrum after ions have left the drift cell. The neutral reactant H_2O enters the equation as the water pressure $p(H_2O)$:

$$K_{eq} = \frac{[(\text{argOMe})H^+ \cdot (H_2O)_n]}{[(\text{argOMe})H^+ \cdot (H_2O)_{n-1}]\, p(H_2O)} \quad (6)$$

The presence of an equilibrium is confirmed by verifying that mass spectra recorded at different drift voltages (resulting in different drift times) are identical. Measuring K_{eq} as a function of temperature and generating a van't Hoff plot (Fig. 10) results in values of $\Delta H°$=–9 kcal mol^{-1} and $\Delta S°$=–17 cal mol^{-1} K^{-1} for the reaction (5). These values are relatively small compared to values measured for alkyl amines and other amino acids [63, 64] (Table 1) indicating that water binds less strongly to a guanidinium group than to an ammonium group. This can be rationalized by the fact that the charge is more delocalized in the larger guanidinium group.

The water binding energy of protonated arginine is measured [62] to be very similar to that of (argOMe)H$^+$ (Table 1) suggesting that argH$^+$ is not a zwitterion. If it were, the H_2O molecule would most probably make as strong a bond to the protonated amine as it does with the simple alkyl amines and with pro and val. Instead, a weak bond is observed indicating the water binds to a protonated arginine side chain. The issue is somewhat ambiguous, however, because if there is a zwitterion the deprotonated carboxylate group could potentially reduce the

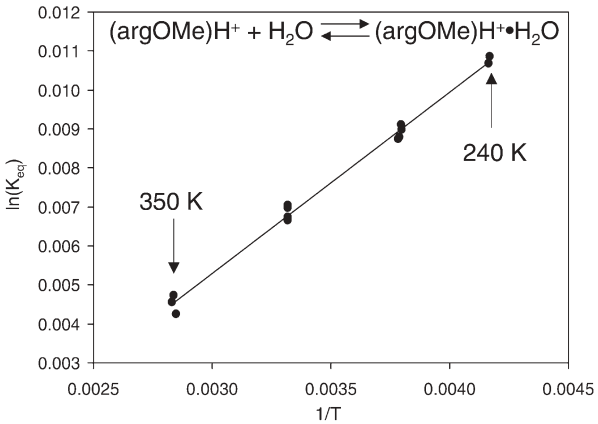

Fig. 10. Van't Hoff plot for the addition of one water molecule to protonated arginine methyl ester

Table 1. Standard enthalpy and entropy of hydration for the protonated species indicated

	$-\Delta H°$ (kcal mol^{-1})	$-\Delta S°$ (cal mol^{-1} K^{-1})
Alkyl amines [64]	~16	~23
pro [63]	18.9	36.8
val [63]	19.3	36.3
arg [62]	9.0	15.4
argOMe [62]	9.2	17.2

amount of positive charge on the amine and therefore reduce the water binding energy of that binding site. Calculations need to be done to draw unambiguous conclusions.

Whatever the detailed interpretation of these results may be in this particular case, the point to make here is that the ion mobility setup provides the opportunity to obtain true thermochemical data, as experiments are carried out under thermal equilibrium conditions.

5
Overview of Applications

5.1
Conformations of Flexible Molecules

For sufficiently small flexible molecules conformational space is fairly limited and only a small number of conformations are energetically reasonable, which makes interpretation of ion mobility data in these cases generally straightforward. If multiple peaks are observed in the ion arrival time distribution (ATD), structural assignment of the peaks is usually unambiguous with help of model structures. If two peaks are present at a given temperature, it can be concluded that the energy barrier between the corresponding two conformations is high compared to the thermal energy available to the molecule. If the two peaks melt into one at higher temperatures, temperature dependent studies can be used to determine the barrier height. Examples for such small flexible molecules with a small number of resolved conformations are oligomers of relatively rigid units. Examples in the literature of this type of systems are the di- and trinucleotides [65] and the trimer of PET (see also Sect. 4.2.3) [60, 61].

A common structural motif of flexible small and medium sized systems, such as synthetic polymers and peptides, is that the charge carrying unit (alkali ion or protonated group) is buried in the interior of the molecule and is well self-solvated by electron rich functional groups [12, 66–71]. As systems get larger multiple shells of self-solvation are observed yielding globular molecular shapes [72]. Functional groups in the second solvation shell are not as tightly bound to the charged center and undergo a fair amount of thermal motion. This is clearly observed as an increase in cross section when temperatures are raised by several 100 K above room temperature [70]. In certain cases structural motifs other than charge solvation can become predominant once the first solvation shell is filled. For instance, in cationized poly(styrene) oligomers two benzene rings fully solvate the metal cation [73]. The remaining benzene rings stack up on top of each other, giving the molecule a distinct "secondary" structure other than spherical. Another very nice example, where maximizing charge solvation is not the only geometry determining factor, is α-helix formation in peptides (10–20 amino acids). In this case hydrogen bonding, alignment of the helix dipole with the charge, and sterical effects are the driving forces for secondary structure formation [74, 75].

Exploring α-helix formation as a function of peptide primary structure enabled Jarrold and coworkers to establish intrinsic helix propensity data for a

number of amino acids [76]. Using these data peptides could be designed where the globular charge solvation structure is comparable in stability to the α-helix [77–79]. Temperature dependent studies on these systems allowed examination of the helix–globule transition and determination of the corresponding barrier height. These studies also showed that there is an intermediate in the transition, possibly a helix, which is less tightly twisted than the α-helix [78].

For larger peptides (~30 amino acids) secondary as well as tertiary structure can be observed. For $ala_nH_3^{3+}$ (n=25–35) two helical sections connected by a loop appear to form an antiparallel helical bundle [80].

Another structural motif, the zwitterion, is potentially present in molecules that contain both acidic and basic functional groups, a situation present in many biomolecules [81–90]. However, zwitterions are intrinsically not stable (for common acids and bases) and require a large amount of stabilization by (self-) solvation and Coulomb interaction with other charges. Zwitterions and non-zwitterions of flexible molecules sometimes assume sufficiently different geometries that the ion mobility technique can be used to distinguish between the two forms. The best examples reported to date are the sodiated oligoglycines that were found not to be zwitterions [91].

Ion mobility data have been obtained for peptide aggregates $(nM+zH)^{z+}$, that are formed in electrospray ionization sources [22, 55–59]. Multimers of larger helical peptides show interesting tertiary structure [58, 59]. In the $Ac–lysH^+–ala_{19}$ dimer the charge of one peptide stabilizes the helix of the other in a head to toe fashion, yielding a helical bundle. However, in the $Ac–ala_{19}–lysH^+$ dimer favorable interaction of the charge of one unit with the helix of the other unit leads to a nearly collinear or vee-shaped arrangement of the two peptides [58]. A similar situation is found in the $Ac–(gly–ala)_7–lysH^+$ dimer and trimer. In the trimer the three charges are in the center and the three helices extend outwards away from each other forming an interesting pinwheel structure [59].

The largest molecules studied by the ion mobility technique to date are proteins with masses of up to ~15,000 u [92–102]. The most thoroughly studied protein is cytochrome *c* where a number of folded and unfolded structures have been observed [92–95]. Ion mobility data suggests that the most tightly folded structures, observed for the low charge states (≤+5), are very similar to the native structure and that the unfolded structures (charge states ~10–15) agree with structures where the tertiary structure is lost, but most of the secondary structure is in place. The highest charge states (~+20) are very stretched out and essentially no secondary structure is present. Unfolding of the protein has been followed for the charge states +5 and +6 by raising the temperature from 300 to near 600 K. A series of transitions is observed in this temperature range from near fully folded at 300 K (cross section of ~1100 Å^2) to substantially unfolded (~2000 Å^2) above 500 K. Other proteins that show multiple conformations include ubiquitin [99–101], lysozyme [98], and apomyoglobin [96, 97]. BPTI, on the other hand, is a protein tied together by three covalent disulfide bridges and only one compact structure is observed in ion mobility experiments [95].

In our lab we have looked at calmodulin, a 146 residue protein involved in calcium regulation. This protein also shows multiple conformations at low charge states (Fig. 11) and has the interesting property that essentially identical cross

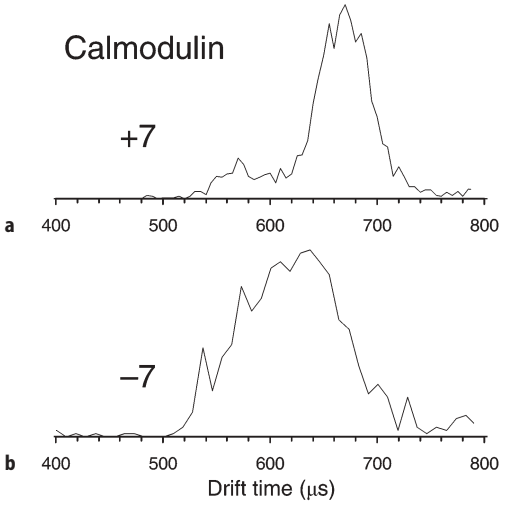

Fig. 11a,b. Ion arrival time distributions of charge states +7 and –7 of the calcium-free protein calmodulin (T=300 K, p=4.9 torr, V_D=90 V, drift length 4.5 cm). For +7 two distinctly different families of structures are present, one with larger cross sections (main peak) and one with smaller cross sections (shoulder to the left). The broad peak for –7 indicates an even distribution of structures with smaller and larger cross sections

sections are observed for equivalent charge states of negative and positive ions [102]. Modeling needs to be done to understand these results, but that is not a simple task for a protein this size.

The study of hydrated biomolecules has only just begun and very few papers have been published on that topic [103–107]. Hydration enthalpies and entropies for the peptides LHRH and bradykinin [108] and for the protein BPTI [106, 107] have been measured and the amount of water addition to folded vs unfolded states of cytochrome *c* has been studied [103–105]. At this point it is too early to draw general conclusions but it is already apparent that only a few water molecules can have significant structural consequences [107, 108].

Adding deuterated water to the ion mobility cell induces H/D-exchange of labile hydrogen atoms in the ion, similar to H/D-exchange observed in FT-ICR mass spectrometers [109–116]. However, this type of ion mobility application has not been widely used. The method has been demonstrated for cytochrome *c* [94, 117], but it is not clear how useful the technique will generally be to obtain structural information of ions.

5.2
Geometries of Clusters

The first applications of ion mobility methods to obtain structural information of polyatomic ions were on cluster ions, that is carbon [1–5] and silicon [6, 7] cluster ions. In carbon clusters atoms are bound to each other by covalent bonds, leading to structures like chains for small clusters (≤10 atoms), rings, polycyclic

planar and cup shaped structures, and cage structures, the fullerenes for larger clusters (>30 atoms). Carbon clusters were still an area of active research during the last five years and new and more complex structures have been found, predominantly due to increased ion mobility resolution [118–123]. New structures include possible intermediates for fullerene formation, as well as multimers of C_{60} fullerene. For instance, for fullerene dimers multiple geometries of fused monomer cage units have been found including two cages connected by a chain [121–123]. Recent work on carbon based cage structures also include studies on silicon, niobium, and scandium containing clusters SiC_n^+, $Nb_xC_{60}^+$ (x=1–5), and $Sc_xC_n^+$ (x=1–3). The SiC_n^+ clusters form virtually identical clusters like C_n^+ except that one carbon atom is replaced by a silicon atom [124]. The $Nb_xC_{60}^+$ clusters are composed of a fullerene C_{60} cage coated by a Nb_x cluster, which can be annealed to $Nb_{x-1}(Nb@C_{60})^+$, a cluster with one Nb atom in the interior of the C_{60} cage [125]. In the ScC_n^+ (n~80) fullerene clusters Sc sits in the interior of the C_n cage [126]. The $Sc_2C_n^+$ clusters show two different structures, one where Sc_2 is inside the C_n cage and one where scandium carbide Sc_2C_2 is inside a C_{n-2} cage. Similarly, the $Sc_3C_n^+$ mobilities agree with a $(Sc_3C_2)@C_{n-2}^+$ structure.

Clusters of the semiconductor elements Si and Ge are much more dense than carbon clusters, but they are not spherical, either, as expected for closed packed atomic spheres. Si_n^+ and Ge_n^+ clusters are prolate with geometries based on stacked tricapped trigonal prisms [127–131]. At a certain cluster size (n~25 for Si_n^+) a structural transition occurs from prolate (n<25) to near spherical (n>25). Interestingly, clusters of tin, which is a metal at room temperature, exhibit very similar structures as Si and Ge, indicating that they are semiconductors as well [131, 132]. Bulk Sn does have a semiconductor form (α-tin), that has the same diamond lattice as Si and Ge. Typical metal clusters appear to pack as tightly as possible and exhibit near spherical shapes as observed for the lead [131, 133], indium [134], and gold [135] clusters. However, the smaller gold clusters Au_n^+ (n≤7) are completely planar [135].

Another class of systems studied by ion mobility is salt clusters, $(NaCl)_nCl^-$ (n<50) [136, 137]. Steps in the ion mobility values as a function of n indicate completion of the 4×3×3, 4×4×3, 4×4×4, and 5×4×4 cuboids. For n>30 several isomers are observed at room temperature, which can be assigned to near cubic and more planar or elongated geometries. At 70°C the less cubic geometries anneal into cuboids with activation barriers of <0.6 eV.

Recent hydration studies of small $(NaI)_nNa^+$ clusters (n=1, 2) indicate that dissociation of $[(NaI)_nNa^+](H_2O)_x$ into $Na^+(H_2O)_y$ ("dissolution") occurs readily at room temperature for x≥6 when n=1 and x≥1 when n=2 [138]. For $[(NaI)Na^+](H_2O)_x$ theory indicates that at least four water molecules are required to solvate one Na^+ ion and form a contact ion pair (i.e., loosen it from the remaining NaI molecule). However, two additional water molecules (six in total) are required to make the $Na^+(H_2O)_4{\cdot}NaI(H_2O)_{x-4}$ cluster a candidate for dissociation under typical experimental conditions [138].

Finally, some ion mobility data is available for a number of clusters composed of an ion and small neutral molecules. Such clusters include $H_3O^+(H_2O)_3$, $NH_4^+(NH_3)_n$, n=1–3, $NO^+(CH_3COCH_3)_n$, n=2, 3 [139–141], complexes between protonated amines and polyethers [21], and ligated transition metal ions

[142–150]. The most unusual geometries among these types of clusters are clearly the multiple-decker sandwich structures observed for vanadium ion-benzene clusters $V_n(C_6H_6)_m^+$ [142, 151–157]. One interesting finding is that "early" transition metals all appear to form sandwich compounds with benzene but for the late metals the benzene adducts coat a central metal cluster [158].

Ligated transition metal ions have been extensively studied by Bowers and coworkers by measuring ligand – metal binding energies $\Delta H°$ and entropies $\Delta S°$ (as in Sect. 4.3) [143–149]. If $\Delta H°$ and $\Delta S°$ values are studied as a function of number of ligands added, important information about the electronic structure of the metal center, the arrangement of the ligands, and ligand sigma bond activation can be obtained. For instance, the Fe^+–(CH_4) bond is relatively weak (18 kcal mol^{-1}) compared to the bond energy of the second methane in the $Fe^+(CH_4)_2$ cluster (26 kcal mol^{-1}), indicating that there is a spin change in the Fe^+ ion upon addition of the first ligand requiring a substantial promotion energy [143]. Large binding entropies (~20 cal mol^{-1} K^{-1}) for the first four CH_4 ligands of Fe^+ and Ni^+ and small values (~10 cal mol^{-1} K^{-1}) for the fifth and sixth ligand give information about how the ligands are arranged: four ligands in the first solvation shell and the fifth and higher in a second shell [143]. This conclusion based on entropy data is consistent with very small binding energies measured for the fifth and sixth ligands (~2 kcal mol^{-1}).

Sigma bond activation is observed in several cases for ligands bound to transition metals. For instance, on the basis of binding energy patterns and supporting calculations it was found that H_2 bound to Zr^+ has an H–Zr^+–H structure, where the Zr^+ ion inserted into the H–H sigma bond [149]. The following two H_2 ligands in $(H–Zr^+–H)(H_2)_2$ bind as H_2 molecules. Interestingly uninsertion is observed when more ligands are added yielding $Zr^+(H_2)_n$ clusters for n>4. Sigma bond activation is also observed for hydrocarbon molecules bound to transition metals as in $Co^+(CH_4)_n$, $Ti^+(CH_4)_n$, $Ti^+(C_2H_4)$, $V^+(C_2H_4)$, $Ti^+(C_3H_8)$, $V^+(C_3H_8)$ [159–163], and interestingly for clusters of B^+ [164] and possibly Al^+ [165].

6 Conclusions

We have shown that combining ion mobility spectrometry (IMS) equipment with mass spectrometry (MS) provides a powerful tool to examine the three-dimensional structure of polyatomic ions by measuring collision cross sections of mass identified ions. The technique is particularly useful in conjunction with molecular modeling or electronic structure calculations. Further, we have reviewed applications where the IMS-MS equipment is used to obtain kinetic and thermochemical data of ions.

IMS-MS applications published in the literature can be grouped into two categories. The first contains studies of conformations of flexible molecules. Such flexible molecules include synthetic polymers and biopolymers such as peptides, proteins, and oligonucleotides. The studies of the second category deal with the geometry of cluster ions such as carbon clusters, semiconductor clusters, metal clusters, salt clusters, ion-ligand clusters. The major conclusions regarding structure of these systems are reviewed in Sect. 5.

Acknowledgements. The support of the Air Force Office of Scientific Research under grant F49620–99–1-0048 and the support of the National Science Foundation under grant CHE-0140215 are gratefully acknowledged. The authors would also like to thank their coworkers at UCSB: Dr. P.R. Kemper, Dr. M. Witt, Dr. P. Barran, Mr. Q. Zhang, Ms. S. Bernstein, and Mr. D.F. Liu for supplying unpublished data presented in this review.

7 References

1. Von Helden G, Hsu MT, Kemper PR, Bowers MT (1991) J Chem Phys 95:3835
2. Von Helden G, Hsu MT, Kemper PR, Bowers MT (1992) Novel forms of carbon. MRS Symposium Series. 270:117
3. Von Helden G, Kemper PR, Gotts NG, Bowers MT (1993) Science 259:1300
4. Von Helden G, Hsu MT, Gotts NG, Kemper PR, Bowers MT (1993) Chem Phys Lett 204:15
5. Von Helden G, Gotts NG, Bowers MT (1993) J Am Chem Soc 115:4363
6. Jarrold MF, Constant VA (1991) Phys Rev Lett 67:2994
7. Jarrold MF, Bower JE (1992) J Chem Phys 96:9180
8. Clemmer DE, Jarrold MF (1997) J Mass Spectrom 32:577
9. Mason EA, McDaniel EW (1988) Transport properties of ions in gases. Wiley, New York
10. Wyttenbach T, von Helden G, Batka JJ, Carlat D, Bowers MT (1997) J Am Soc Mass Spectrom 8:275
11. Wyttenbach T, Witt M, Bowers MT (2000) J Am Chem Soc 122:3458
12. Gidden J, Jackson AT, Scrivens JH, Bowers MT (1999) Int J Mass Spectrom 188:121
13. Mesleh MF, Hunter JM, Shvartsburg AA, Schatz GC, Jarrold MF (1996) J Phys Chem 100:16,082
14. Shvartsburg AA, Jarrold MF (1996) Chem Phys Lett 261:86
15. Shvartsburg AA, Liu B, Jarrold MF, Ho KM (2000) J Chem Phys 112:4517
16. Case DA, Pearlman DA, Caldwell JW, Cheatham TE III, Ross WS, Simmerling CL, Darden TA, Merz KM, Stanton RV, Cheng AL, Vincent JJ, Crowley M, Tsui V, Radmer RJ, Duan Y, Pitera J, Massova I, Seibel GL, Singh UC, Weiner PK, Kollman PA (1999) AMBER 6. University of California, San Francisco
17. Gidden J, Kemper PR, Shammel E, Fee DP, Anderson S, Bowers MT (2003) Int J Mass Spectrom 222:63
18. Shammel E, Gidden J, Fee DP, Kemper PR, Anderson S, Bowers MT (2003) Int J Mass Spectrom 222:63
19. Hoaglund-Hyzer CS, Clemmer DE (2001) Anal Chem 73:177
20. Hoaglund CS, Valentine SJ, Clemmer DE (1997) Anal Chem 69:4156
21. Creaser CS, Griffiths JR, Stockton BM (2000) Eur J Mass Spectrom 6:213; Creaser CS, Benyezzar M, Griffiths JR, Stygall JW (2000) Anal Chem 72:2724
22. Wyttenbach T, Kemper PR, Bowers MT (2001) Int J Mass Spectrom 212:13
23. Nestler V, Betz B, Warneck P (1977) Ber Bunsen Phys Chem 81:13
24. Thomas R, Barassin A, Burke RR (1978) Int J Mass Spectrom 28:275
25. Johnson R, Biondi MA, Hayashi M (1982) J Chem Phys 77:2545
26. Bohringer H, Arnold F (1983) Int J Mass Spectrom 49:61
27. Kaneko Y, Megill LR, Hasted JB (1966) J Chem Phys 45:3741
28. Federer W, Ramler H, Villinger H, Lindinger W (1985) Phys Rev Lett 54:540
29. Twiddy ND, Mohebati A, Tichy M (1986) Int J Mass Spectrom 74:251
30. Adams NG, Smith D (1988) Adv At Mol Phys 23:1
31. Viggiano AA, Morris RA, Dale F, Paulson JF, Giles K, Smith D, Su T (1990) J Chem Phys 93:1149
32. McEwan MJ (1992) In: Adams NG, Babcock LM (eds) Advances in gas phase ion chemistry. JAI, Greenwich, CT, vol 1, p 1
33. Krishnamurthy M, De Gouw JA, Bierbaum VM, Leone SR (1996) J Phys Chem 100:14,908
34. McFarland M, Albritton DL, Fehsenfeld FC, Ferguson EE, Schmeltekopf AL (1973) J Chem Phys 59:6610

35. Wu C, Siems WF, Asbury GR, Hill HH (1998) Anal Chem 70:4929
36. Dugourd P, Hudgins RR, Clemmer DE, Jarrold MF (1997) Rev Sci Instr 68:1122
37. Kemper PR, Bowers MT (1990) J Am Soc Mass Spectrom 1:197
38. Bluhm BK, Gillig KJ, Russell DH (2000) Rev Sci Instr 71:4078
39. Hoaglund CS, Valentine SJ, Sporleder CR, Reilly JP, Clemmer DE (1998) Anal Chem 70:2236
40. Valentine SJ, Kulchania M, Barnes CAS, Clemmer DE (2001) Int J Mass Spectrom 212:97
41. Steiner WE, Clowers BH, Fuhrer K, Gonin M, Matz LM, Siems WF, Schultz AJ, Hill HH (2001) Rapid Commun Mass Spectrom 15:2221
42. Gillig KJ, Ruotolo B, Stone EG, Russell DH, Fuhrer K, Gonin M, Schultz AJ (2000) Anal Chem 72:3965
43. Stone EG, Gillig KJ, Ruotolo BT, Russell DH (2001) Int J Mass Spectrom 212:519
44. Woods AS, Koomen JM, Ruotolo BT, Gillig KJ, Russel DH, Fuhrer K, Gonin M, Egan TF, Schultz JA (2002) J Am Soc Mass Spectrom 13:166
45. Kemper PR, Bowers MT (2002) Instrumental paper on TOF-drift cell-quad setup (to be published), see also [17, 18]
46. Kemper PR, Bowers MT (1990) J Am Chem Soc 112:3231
47. Matz LM, Asbury GR, Hill HH (2002) Rapid Commun Mass Spectrom 16:670
48. Witt M, Bowers MT. Unpublished results; experimental details as in [11]
49. Gatland IR (1974) In: McDaniel EW, McDowell MRC (eds) Case studies in atomic collision physics. North-Holland, Amsterdam, vol 4, p 369
50. Koch KJ, Gozzo FC, Zhang DX, Eberlin MN, Cooks RG (2001) Chem Commun 1854
51. Cooks RG, Zhang DX, Koch KJ, Gozzo FC, Eberlin MN (2001) Anal Chem 73:3646
52. Counterman AE, Clemmer DE (2001) J Phys Chem B 105:8092
53. Julian RR, Hodyss R, Kinnear B, Jarrold MF, Beauchamp JL (2002) J Phys Chem B 106:1219
54. Wyttenbach T, Barran P, Bowers MT. Unpublished results
55. Counterman AE, Hilderbrand AE, Barnes CAS, Clemmer DE (2001) J Am Soc Mass Spectrom 12:1020
56. Counterman AE, Valentine SJ, Srebalus CA, Henderson SC, Hoaglund CS, Clemmer DE (1998) J Am Soc Mass Spectrom 9:743
57. Lee SW, Beauchamp JL (1999) J Am Soc Mass Spectrom 10:347
58. Hudgins RR, Jarrold MF (1999) J Am Chem Soc 121:3494
59. Kaleta DT, Jarrold MF (2002) J Am Chem Soc 124:1154
60. Gidden J, Wyttenbach T, Batka JJ, Weis P, Jackson AT, Scrivens JH, Bowers MT (1999) J Am Soc Mass Spectrom 10:883
61. Gidden J, Wyttenbach T, Batka JJ, Weis P, Jackson AT, Scrivens JH, Bowers MT (1999) J Am Chem Soc 121:1421
62. Wyttenbach T, Bowers MT. Unpublished results
63. Meot-Ner M, Field FH (1974) J Am Chem Soc 96:3168
64. Blades AT, Klassen JS, Kebarle P (1996) J Am Chem Soc 118:12,437
65. Gidden J, Bushnell JE, Bowers MT (2001) J Am Chem Soc 123:5610
66. von Helden G, Wyttenbach T, Bowers MT (1995) Science 267:1483
67. von Helden G, Wyttenbach T, Bowers MT (1995) Int J Mass Spectrom Ion Proc 146:349
68. Wyttenbach T, von Helden G, Bowers MT (1996) J Am Chem Soc 118:8355
69. Wyttenbach T, von Helden G, Bowers MT (1997) Int J Mass Spectrom Ion Proc165:377
70. Gidden J, Wyttenbach T, Jackson AT, Scrivens JH, Bowers MT (2000) J Am Chem Soc 122:4692
71. Wyttenbach T, Bushnell JE, Bowers MT (1998) J Am Chem Soc 120:5098
72. Hudgins RR, Jarrold MF (2000) J Phys Chem B 104:2154
73. Gidden J, Bowers MT, Jackson AT, Scrivens JH (2002) J Am Soc Mass Spectrom 13:499
74. Hudgins RR, Ratner MA, Jarrold MF (1998) J Am Chem Soc 120:12,974
75. Kohtani M, Kinnear BS, Jarrold MF (2000) J Am Chem Soc 122:12,377
76. Kinnear BS, Jarrold MF (2001) J Am Chem Soc 123:7907
77. Kinnear BS, Hartings MR, Jarrold MF (2002) J Am Chem Soc 124:4422

78. Kinnear BS, Hartings MR, Jarrold MF (2001) J Am Chem Soc 123:5660
79. Kaleta DT, Jarrold MF (2001) J Phys Chem B 105:4436
80. Counterman AE, Clemmer DE (2001) J Am Chem Soc 123:1490
81. Wyttenbach T, Witt M, Bowers MT (1999) Int J Mass Spectrom 183:243
82. Wyttenbach T, Bowers MT (1999) J Am Soc Mass Spectrom 10:9
83. Jockusch RA, Lemoff AS, Williams ER (2001) J Phys Chem A 105:10,929
84. Strittmatter EF, Lemoff AS, Williams ER (2000) J Phys Chem A 104:9793
85. Jockusch RA, Price WD, Williams ER (1999) J Phys Chem A 103:9266
86. Price WD, Jockusch RA, Williams ER (1997) J Am Chem Soc 119:11,988
87. Cerda BA, Wesdemiotis C (2000) Analyst 125:657
88. Talley JM, Cerda BA, Ohanessian G, Wesdemiotis C (2002) Chem Eur J 8:1377
89. Julian RR, Beauchamp JL, Goddard WA (2002) J Phys Chem A 106:32
90. Julian RR, Hodyss R, Beauchamp JL (2001) J Am Chem Soc 123:3577
91. Wyttenbach T, Bushnell JE, Bowers MT (1998) J Am Chem Soc 120:5098
92. Mao Y, Ratner MA, Jarrold MF (1999) J Phys Chem B 103:10,017
93. Mao Y, Woenckhaus J, Kolafa J, Ratner MA, Jarrold MF (1999) J Am Chem Soc 121:2712
94. Valentine SJ, Clemmer DE (1997) J Am Chem Soc 119:3558
95. Shelimov KB, Clemmer DE, Hudgins RR, Jarrold MF (1997) J Am Chem Soc 119:2240
96. Shelimov KB, Jarrold MF (1997) J Am Chem Soc 119:2987
97. Hoaglund-Hyzer CS, Counterman AE, Clemmer DE (1999) Chem Rev 99:3037
98. Valentine SJ, Anderson JG, Ellington AD, Clemmer DE (1997) J Phys Chem B 101:3891
99. Valentine SJ, Counterman AE, Clemmer DE (1997) J Am Soc Mass Spectrom 8:954
100. Li JW, Taraszka JA, Counterman AE, Clemmer DE (1999) Int J Mass Spectrom 187:37
101. Badman ER, Hoaglund-Hyzer CS, Clemmer DE (2002) J Am Soc Mass Spectrom 13 :719
102. Barran P, Wyttenbach T, Bowers MT. Unpublished results
103. Mao Y, Ratner MA, Jarrold MF (2001) J Am Chem Soc 123:6503
104. Fye JL, Woenckhaus J, Jarrold MF (1998) J Am Chem Soc 120:1327
105. Woenckhaus J, Mao Y, Jarrold MF (1997) J Phys Chem B 101:847
106. Woenckhaus J, Hudgins RR, Jarrold MF (1997) J Am Chem Soc 119:9586
107. Mao Y, Ratner MA, Jarrold MF (2000) J Am Chem Soc 122:2950
108. Barran P, Wyttenbach T, Bernstein S, Liu DF, Bowers MT. To be published; Liu D, Wyttenbach T, Barran PE, Bowers MT (2003) J Am Chem Soc (submitted)
109. Schlosser M, Mongin F, Porwisiak J, Dmowski W, Buker HH, Nibbering NMM (1998) Chem Eur J 4:1281
110. Nourse BD, Hettich RL, Buchanan MV (1993) J Am Soc Mass Spectrom 4:296
111. Lee SW, Lee HN, Kim HS, Beauchamp JL (1998) J Am Chem Soc 120:5800
112. Winger BE, Lightwahl KJ, Rockwood AL, Smith RD (1992) J Am Chem Soc 114:5897
113. Freitas MA, Marshall AG (2001) J Am Soc Mass Spectrom 12:780
114. McLafferty FW, Guan ZQ, Haupts U, Wood TD, Kelleher NL (1998) J Am Chem Soc 120:4732
115. Green MK, Lebrilla CB (1998) Int J Mass Spectrom Ion Proc 175:15
116. Zhang X, Ewing NP, Cassady CJ (1998) Int J Mass Spectrom Ion Proc 175:159
117. Valentine SJ, Clemmer DE (2002) J Am Soc Mass Spectrom 13:506
118. Dugourd P, Hudgins RR, Tenenbaum JM, Jarrold MF (1998) Phys Rev Lett 80:4197
119. Shvartsburg AA, Schatz GC, Jarrold MF (1998) J Chem Phys 108:2416
120. Shvartsburg AA, Hudgins RR, Dugourd P, Gutierrez R, Frauenheim T, Jarrold MF (2000) Phys Rev Lett 84:2421
121. Shvartsburg AA, Hudgins RR, Gutierrez R, Jungnickel G, Frauenheim T, Jackson KA, Jarrold MF (1999) J Phys Chem A 103:5275
122. Shvartsburg AA, Pederson LA, Hudgins RR, Schatz GC, Jarrold MF (1998) J Phys Chem A 102:7919
123. Shvartsburg AA, Hudgins RR, Dugourd P, Jarrold MF (1997) J Phys Chem A 101:1684
124. Fye JL, Jarrold MF (1997) J Phys Chem A 101:1836
125. Fye JL, Jarrold MF (1999) Int J Mass Spectrom 187:507

126. Sugai T, Inakuma M, Hudgins R, Dugourd P, Fye JL, Jarrold MF, Shinohara H (2001) J Am Chem Soc 123:6427
127. Hudgins RR, Imai M, Jarrold MF, Dugourd P (1999) J Chem Phys 111:7865
128. Shvartsburg AA, Liu B, Lu ZY, Wang CZ, Jarrold MF, Ho KM (1999) Phys Rev Lett 83:2167
129. Liu B, Lu ZY, Pan BC, Wang CZ, Ho KM, Shvartsburg AA, Jarrold MF (1998) J Chem Phys 109:9401
130. Ho KM, Shvartsburg AA, Pan BC, Lu ZY, Wang CZ, Wacker JG, Fye JL, Jarrold MF (1998) Nature 392:582
131. Shvartsburg AA, Hudgins RR, Dugourd P, Jarrold MF (2001) Chem Soc Rev 30:26
132. Shvartsburg AA, Jarrold MF (1999) Phys Rev A 60:1235
133. Shvartsburg AA, Jarrold MF (2000) Chem Phys Lett 317:615
134. Lerme J, Dugourd P, Hudgins RR, Jarrold MF (1999) Chem Phys Lett 304:19
135. Gilb S, Weis P, Furche F, Ahlrichs R, Kappes MM (2002) J Chem Phys 116:4094
136. Hudgins RR, Dugourd P, Tenenbaum JM, Jarrold MF (1997) Phys Rev Lett 78:4213
137. Dugourd P, Hudgins RR, Jarrold MF (1997) Chem Phys Lett 267:186
138. Zhang Q, Carpenter CJ, Kemper PR, Bowers MT (2003) J Am Chem Soc (in press)
139. Krishnamurthy M, deGouw JA, Ding LN, Bierbaum VM, Leone SR (1997) J Chem Phys 106:530
140. de Gouw JA, Krishnamurthy M, Bierbaum VM, Leone SR (1997) Int J Mass Spectrom Ion Proc 167:281
141. de Gouw JA, Ding LN, Krishnamurthy M, Lee HS, Anthony EB, Bierbaum VM, Leone SR (1996) J Chem Phys 105:10,398
142. Weis P, Kemper PR, Bowers MT (1997) J Phys Chem A 101:8207
143. Zhang Q, Kemper PR, Bowers MT (2001) Int J Mass Spectrom 210:265
144. Kemper PR, Weis P, Bowers MT, Maitre P (1998) J Am Chem Soc 120:13,494
145. Kemper PR, Weis P, Bowers MT (1998) Chem Phys Lett 293:503
146. Bushnell JE, Maitre P, Kemper PR, Bowers MT (1997) J Chem Phys 106:10,153
147. Kemper PR, Weis P, Bowers MT (1997) Int J Mass Spectrom Ion Proc 160:17
148. Weis P, Kemper PR, Bowers MT (1997) J Phys Chem A 101:2809
149. Bushnell JE, Kemper PR, van Koppen P, Bowers MT (2001) J Phys Chem A 105:2216
150. Leavell MD, Gaucher SP, Leary JA, Taraszka JA, Clemmer DE (2002) J Am Soc Mass Spectrom 13:284
151. Judai K, Sera K, Amatsutsumi S, Yagi K, Yasuike T, Yabushita S, Nakajima A, Kaya K (2001) Chem Phys Lett 334:277
152. Kurikawa T, Takeda H, Hirano M, Judai K, Arita T, Nagao S, Nakajima A, Kaya K (1999) Organometallics 18:1430
153. Yasuike T, Nakajima A, Yabushita S, Kaya K (1997) J Phys Chem A 101:5360
154. Kurikawa T, Takeda H, Nakajima A, Kaya K (1997) Z Phys D Atom Mol Clusters 40:65
155. Hoshino K, Kurikawa T, Taked AH, Nakajima A, Kaya K (1996) Surf Rev Lett 3:183
156. Kurikawa T, Hirano M, Taked AH, Yagi K, Hoshino K, Nakajima A, Kaya K (1995) J Phys Chem 99:16,248
157. Hoshino K, Kurikawa T, Taked AH, Nakajima A, Kaya K (1995) J Phys Chem 99:3053
158. Kemper PR, Bowers MT. Unpublished results
159. Zhang Q, Kemper PR, Shin SK, Bowers MT (2001) Int J Mass Spectrom 204:281
160. Carpenter CJ, van Koppen PAM, Bowers MT, Perry JK (2000) J Am Chem Soc 122:392
161. van Koppen PAM, Perry JK, Kemper PR, Bushnell JE, Bowers MT (1999) Int J Mass Spectrom 187:989
162. van Koppen PAM, Bowers MT, Haynes CL, Armentrout PB (1998) J Am Chem Soc 120:5704
163. Gidden J, van Koppen PAM, Bowers MT (1997) J Am Chem Soc 119:3935
164. Kemper PR, Bushnell JE, Weis P, Bowers MT (1998) J Am Chem Soc 120:7577
165. Kemper PR, Bushnell J, Bowers MT, Gellene GI (1998) J Phys Chem A 102:8590